ABCM 40 anos
Associação Brasileira de Engenharia e Ciências Mecânicas

CONEM 2016
CONGRESSO NACIONAL DE ENGENHARIA MECÂNICA

21 - 25 AGOSTO DE 2016
FORTALEZA - CEARÁ

AN AERO-PROPULSIVE MODEL OF THE TECHNOLOGICAL DEMONSTRATOR SCRAMJET 14-X S: PRELIMINARY RESULTS

Sebastião de Carvalho Netto, scnetto27@hotmail.com[1]
Paulo Gilberto de Paula Toro, toro@ieav.cta.br[2]
Marco Antônio Sala Minucci, sala@ieav.cta.br[2]
Israel da Silveira Rêgo, israel.rego@ieav.cta.br[2]

[1]Instituto Tecnológico de Aeronáutica (ITA), Praça Marechal Eduardo Gomes, nº 50, Vila das Acácias, CEP 12.228-900, São José dos Campos/SP-Brasil.
[2]Instituto de Estudos Avançados (IEAv), Trevo Coronel Aviador José Alberto Albano do Amarente, nº 1, Putim, CEP 12.228-001, São José dos Campos/SP-Brasil.

Abstract: *Scramjets represents the last frontier in aeronautical high-speed engines. The Aerothermodynamics and Hypersonics laboratory Prof. Henry T. Nagamatsu at the Institute for Advanced Studies (IEAv), is carrying out research and development of technological demonstrators of hypersonic airbreathing propulsion based on supersonic combustion. One of them is the scramjet 14-X S that will be tested in flight at 30 km altitude and speed equivalent to Mach 7, as an airbreathing third-stage rocket engine for access to space. The 14-X S scramjet is an engine with planar symmetry, where each half has two compression ramps (inlet), a combustion chamber (combustor) and two expansion surfaces (nozzle) for thrust generation. This article presents ananalytical model for the determination of the aerodynamics forces (drag & lift) and the propulsive force (thrust) that act on the 14-X S in atmospheric hypersonic flight. The aero-propulsive model proposed herein considers air as a calorically perfect gas, standard atmosphere for freestream, shock wave theory to determine the angle of the shocks generated by the inlet of the 14-X S and the properties through them, theory of Rayleigh to estimate the heat addition from combustion reaction between supersonic stream of air and hydrogen in the combustor, isentropic expansion theory (area ratio) to calculate the properties of the exhaustion through confined regions, Prandtl-Meyer theory to obtain the airflow properties through centered expansion waves, and finally thrust calculation. The effect of viscosity was considered by changing the geometry of the inlet and the nozzle of 14-X S, and thereby, the shock and expansion angles, while the friction was determined from Van Driest solutions for laminar flow. The preliminary calculation shows the following results: The pressure drag is maximum on the second compression ramp of the 14-X S; the friction is more pronounced along the first expansion section; the 14-X S main body creates more drag than its cowl; the overall wave drag on the 14-X S flight model is greater than the total friction; the longitudinal thrust generated is such that produces a small net deceleration of the 14-X S;*

Palavras-chave: *scramjet, aerodynamic loads, thrust,hypersonic, flight test*

1. INTRODUCTION

The Laboratory Professor H. T. Nagamatsu bellowing to the Division of Aerothermodynamics and Hypersonic of the Institute for Advanced Studies (IEAv) in Brazil is developing hypersonic Airbreathing propulsion systems (scramjet engines based on supersonic combustion) under the 14-X flight research project for safe, cheap and “green” access to space (Toro *et al.*, 2012). The primary objective of the 14-X project is to demonstrate in flight the operation of a scramjet engine powered by hydrogen fuel at hypervelocities. Additional objectives include achieving net acceleration during the scramjet propulsion and obtaining flight data on aerothermodynamics. This paper reports on the calculations of aerodynamic forces (drag and lift) and longitudinal thrust generated by the 14-X S scramjet engine, which is a technological demonstrator of an airbreathing third-stage rocket engine powered by H_2 fuel for atmospheric flight in the stratosphere at speed equivalent to Mach number 7. Next, an aero-propulsive model for calculating such force is suggested, followed by the initial results and conclusions.

2. METHODOLOGY

2.1. Freestream Conditions

The atmospheric properties found by 14-X S at Mach 7 in the atmosphere at 30 km altitude were obtained via lapses of temperature and exponential model pressure; the viscosity and thermal conductivity were obtained by Sutherland law according to Eqs (1) and (2), respectively; and the speed of sound and of flow at Mach 7 by Eqs (3) and (4) respectively, what is called design conditions, whose values are presented in Tab. 1.

$$\mu = \frac{1,458 \times 10^{-6} \times T^{3/2}}{T + 110,4} \tag{1}$$

$$k = \frac{1,99 \times 10^{-3} \times T^{3/2}}{T + 112} \tag{2}$$

$$a = \sqrt{\gamma R T} \tag{3}$$

$$u = Ma \tag{4}$$

Table 1. Freestream conditions for the 14-X S flight test.

Mach	u [m/s]	p [Pa]	T [K]	a [m/s]	ρ [kg/m^3]	μ [kg/s.m]	k [J/s.m.K]
7,0	2.135,6	1.158,6	231,7	305,1	0,017	1,503E-5	2,042E-2

2.2. 14-X S Flight Model

The 14-X S (Fig. 1) is symmetrical version of the 14-X B (Fig. 2) whose geometry enables to calculate the variations in properties and direction of flow on the surfaces of the vehicle (specified in Fig. 3), which will be under effects of compression, combustion and expansion. The main dimensions of 14-X S for flight test are classified and cannot be shown herein.

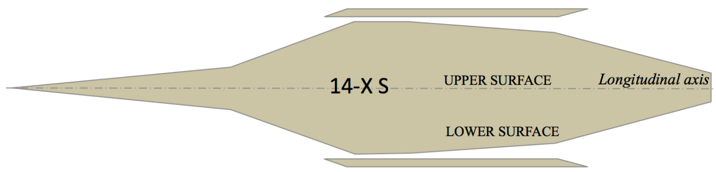

Figure 1. Scheme of the 14-X S as longitudinal mirroring of the 14-XB.

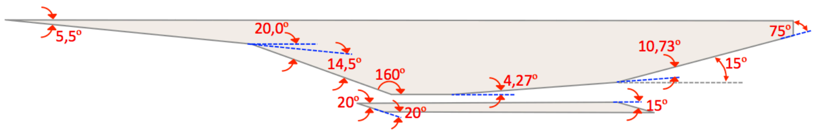

Figure 2. Geometry of the 14-XB.

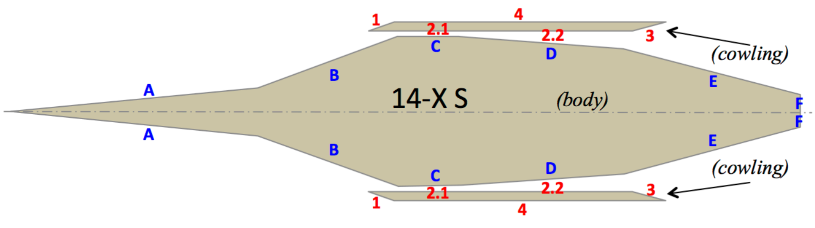

Figure 3. Definition of the surfaces of the vehicle (body and cowling) to calculate the flow properties.

In order to structural integrity, in its flight version, the 14-X S will be their lateral ends closed by two identical plates, as shown in Fig. 4.

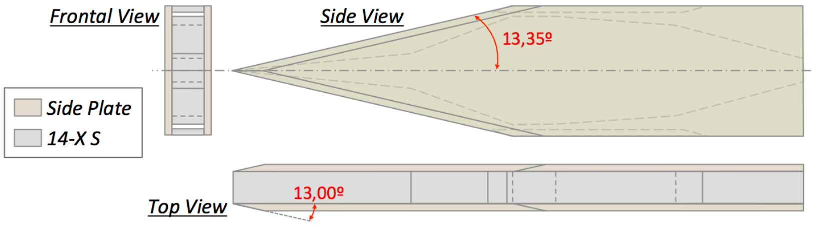

Figure 4. Geometry of the side plates and mounting layout in 14-X S, 3 views.

The Fig. 5 highlights the internal areas of the side plates that are under the influence of the inner flow along each body section, as well as the internal area, which is under the influence of the freestream.

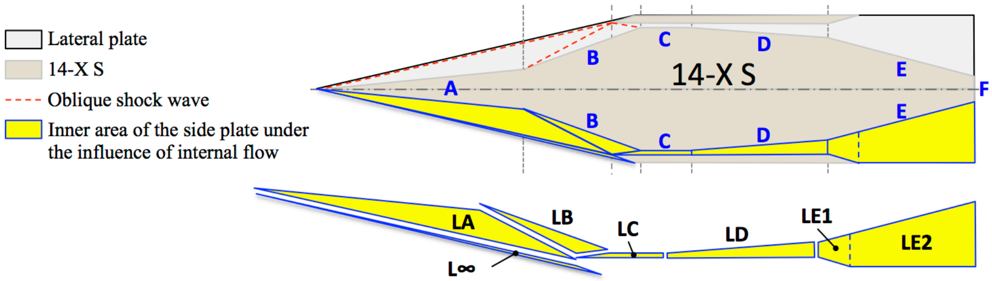

Figure 5. Inner regions of the side plates under the influence of the internal flow (on each section).

The Fig. 6 highlights the outer areas of the side plates that are under the influence of freestream and subsequent expansions and compressions.

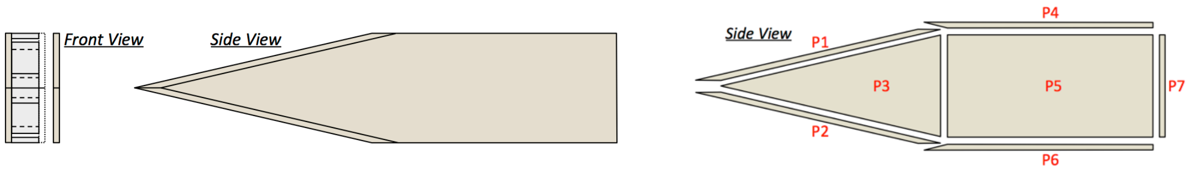

Figure 6. Outer regions of the side plates under the influence of freestream and subsequent compressions and expansions.

2.3. Assumptions and Simplifications

Air is considered as a calorically perfect gas, i.e., the ratio of specific heats at constant pressure and volume, γ is assumed to be constant and equal to 1,4, as well as the constant of air R, which is considered constant and equal 287 J/kg.K. Also, the 14-X S it was assumed in level flight, with null angles of attack and yaw.

Initially, it is considered non-viscous flow, no combustion (without the addition of heat, power-off) and, in sequence, there was obtained the properties with the heat addition (combustion, without taking into mass addition regard products of reaction). Then, it considered the effects of viscosity (existence of the boundary layer) without the heat addition and, in sequence, is computed the properties of viscous flow condition and with the addition of heat (power-on).

In the case of viscous flow were used the solutions for laminar boundary layer from Van Driest (1952) for obtaining the friction coefficients (c_f), the shear stresses on the walls (τ_w), and the maximum thickness of boundary layers; all obtained depending on the Mach and Reynolds numbers of freestream on the section being analyzed, always with the case where the temperature of the wall is equal to the flow temperature at the edge of the boundary layer. It is important to note that the thickness of the boundary layer increases linearly from the beginning of a given section to its end and that its growth rate accompanies the variation of the freestream properties of the section where the layer develops. Moreover, it is not considered any interaction of shock-boundary layer.

It is known that the existence of the boundary layer leads to a virtual change in inclination of each section, and therefore, it is computed again flow properties for each section taking into account these virtual inclinations. However, in the combustor, the boundary layer is considered only to obtain the viscous drag, be fully discharged for calculating of the heat addition, keeping assumption of the one-dimensional flow with constant area, or Rayleigh flow.

In cases where it was considered combustion, was obtained flow properties after adding of the heat via the Rayleigh flow (one-dimensional flow with the addition of heat and constant area) and, with these, computed the maximum amount of heat added, specific and absolute, by complete combustion of air and hydrogen (η_b = 1) for non-choke of the scramjet (Mach 1) - resulting in a poor mixture of fuel. Still, it was considered the condition of shock on-lip-on-corner, i.e., perfect focus of the first two shocks on the edge (leading edge) of the cowling and subsequent reflection on the combustor inlet, so that all the mass of air that passes through the three shocks is admitted to the combustor (Fig. 7).

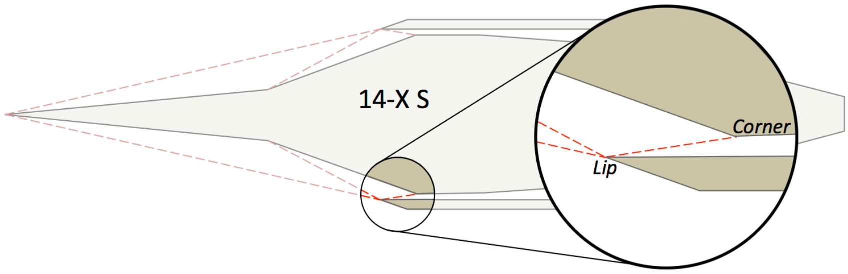

Figure 7. Scheme of the shock on-lip-on-corner condition for the optimal capture of air.

For regions under the influence of confined expansion was used quasi-one-dimensional flow (flow in nozzles). The sliding line between the flows arising from section 4 and Freestream, and hot jet (section 3) was considered forming a "virtual" nozzle.

The trailing edge of the 14-S X has an inclination of 90° to the horizontal reference, making it difficult to calculate the pressure through focused expansion. Thus, it was decided to establish a simplistic method for obtaining the pressure in the section F, which was the determination of the average pressure between freestream and section E.

The side plates also contribute to the viscous and wave drags, which were computed, based on the pressure fields and on the shear stress distribution of on the regions of the plates. It should be noted that the Reynolds number was computed using the average length of each region of the plates, shown in Figs. (5) and (6).

2.4. Governing Equations

To determine the flow properties that experience compression, heat adding (combustion) and expansion (confined and free) was used HAP software that accompanies the book Hypersonic Airbreathing Propulsion from Heiser *et al.* (1994). This program allows greater flexibility in the calculation of the flow properties and, among other features, includes the following described theories:

2.4.1. The Oblique Shock Wave Relations

The oblique shock relations for the flow across the oblique shock wave, Eqs. (5) to (11), were obtained applying the following equations: continuity, momentum, energy, and state; considering the enthalpy for ideal gas; and using the indications ***in*** and ***out***, respectively, for the regions upstream and downstream the shock (Fig. 8).

$$M_{n_{in}} = M_{in} \sin\beta \tag{5}$$

$$\frac{\rho_{out}}{\rho_{in}} = \frac{(\gamma+1)M_{n_{in}}^2}{(\gamma-1)M_{n_{in}}^2+2} \tag{6}$$

$$\frac{p_{out}}{p_{in}} = 1+\frac{2\gamma}{(\gamma+1)}(M_{n_{in}}^2-1) \tag{7}$$

$$\frac{T_{out}}{T_{in}} = \frac{p_{out}}{p_{in}}\frac{\rho_{in}}{\rho_{out}} \tag{8}$$

$$M_{n_{out}}^2 = \frac{M_{n_{in}}^2+\left[\frac{2}{\gamma-1}\right]}{\left[\frac{2\gamma}{\gamma-1}\right]M_{n_{in}}^2-1} \tag{9}$$

$$M_{out} = \frac{M_{n_{out}}}{\sin(\beta - \theta)} \tag{10}$$

$$\tan\theta = 2\cot\beta\left[\frac{M_{in}^2 \sin^2\beta - 1}{M_{in}^2(\gamma + \cos 2\beta) + 2}\right] \tag{11}$$

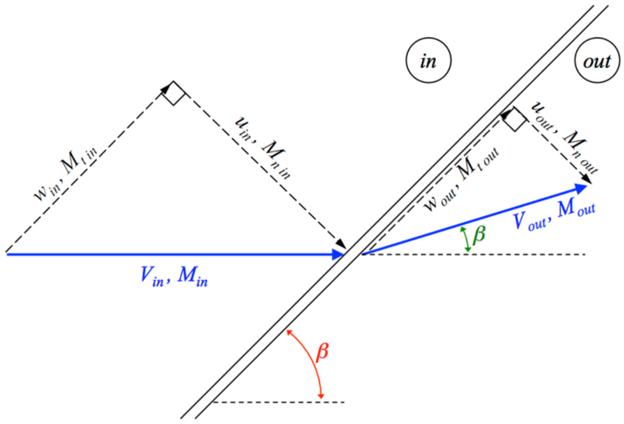

Figure 8. Oblique shock wave geometry (adapted from Anderson, 1990).

2.4.2. One-Dimensional Flow with Heat Addition (Rayleigh's flow)

The Rayleigh relations for a non-adiabatic flow, Eqs. (12) to (17), were obtained by applying the following equations: continuity, momentum, energy, and state; considering enthalpy for ideal gas; assuming one-dimensional flow through a constant area with addition of heat; and using the indices ***in*** and ***out*** for regions prior to and posterior to heat addition (Fig. 9).

$$q = c_p(T_{0out} - T_{0in}) \tag{12}$$

$$\frac{p_{out}}{p_{in}} = \frac{1+\gamma M_{in}^2}{1+\gamma M_{out}^2} \tag{13}$$

$$\frac{T_{out}}{T_{in}} = \left(\frac{1+\gamma M_{in}^2}{1+\gamma M_{out}^2}\right)\left(\frac{M_{out}}{M_{in}}\right)^2 \tag{14}$$

$$\frac{\rho_{out}}{\rho_{in}} = \left(\frac{1+\gamma M_{out}^2}{1+\gamma M_{in}^2}\right)\left(\frac{M_{in}}{M_{out}}\right)^2 \tag{15}$$

$$\frac{p_{0_{out}}}{p_{0_{in}}} = \left(\frac{1+\gamma M_{in}^2}{1+\gamma M_{out}^2}\right)\left(\frac{1+\frac{\gamma-1}{2}M_{out}^2}{1+\frac{\gamma-1}{2}M_{in}^2}\right)^{\gamma/(\gamma-1)} \tag{16}$$

$$\frac{T_{0_{out}}}{T_{0_{in}}} = \left(\frac{1+\gamma M_{in}^2}{1+\gamma M_{out}^2}\right)^2\left(\frac{M_{out}}{M_{in}}\right)^2\left(\frac{1+\frac{\gamma-1}{2}M_{out}^2}{1+\frac{\gamma-1}{2}M_{in}^2}\right) \tag{17}$$

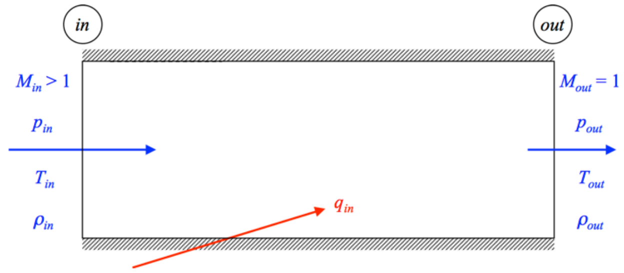

Figure 9. Schematic of quantities for one-dimensional flow with heat addition (adapted from Anderson, 1990).

2.4.3. Heat of Combustion and Fuel Flow Rate

The energy released by the exothermic reactions of combustion, Eq. (18), which is added to the supersonic airflow in the combustor, is expressed as (Heiser *et al.,* 1994):

$$\text{Heat added} = \frac{\eta_b \dot{m}_f h_{PR}}{\dot{m}_0} \tag{18}$$

, where η_b is combustion efficiency, $\dot{m}_f$ is the fuel mass flow rate (kg/s), $\dot{m}_0$ is entry air mass flow rate, and, and h_{PR} is heat of reaction of the H_2 fuel. Equation (12) gives the maximum amount of heat that can be added to the airflow in the combustor without choking it (Mach 1 at the combustor exit), while Eq. (18) gives $\dot{m}_f$ to do so.

2.4.4. Prandtl-Meyer Expansion Waves (Centered Expansion)

The Prandtl-Meyer relations for the flow across an expansion fan, Eqs. (19) and (20), were obtained considering small changes in properties and direction of the flow across Mach waves into the expansion fan, where the indices ***in*** and ***out*** refers to upstream and downstream conditions relative to the expansion fan (Fig. 10).

$$\nu(M) = \sqrt{\frac{\gamma+1}{\gamma-1}} \tan^{-1} \sqrt{\frac{\gamma-1}{\gamma+1}\left(M^2-1\right)} - \tan^{-1}\sqrt{M^2-1} \tag{19}$$

$$\theta_{out} = \nu\left(M_{out}\right) - \nu\left(M_{in}\right) \tag{20}$$

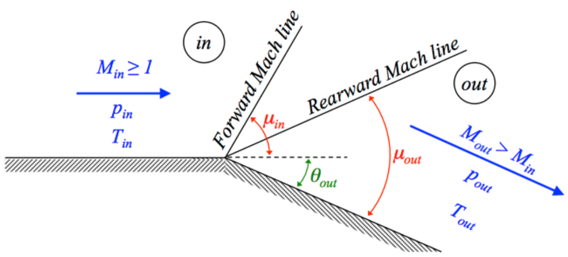

Figure 10. Prandtl-Meyer expansion, or centered expansion (adapted from Anderson, 1990).

2.4.5. Confined Expansion (Nozzle Flow)

Equation (21) is called the area-Mach number relation that governs the confined expansion along a divergent duct (Fig. 11). Such relation is obtained by applying the following equations: continuity, momentum, energy, and state; and assuming isentropic flow acceleration.

$$\left(\frac{A}{A^*}\right)^2 = \frac{1}{M^2}\left[\frac{2}{\gamma+1}\left(1+\frac{\gamma-1}{2}M^2\right)\right]^{(\gamma+1)/(\gamma-1)} \tag{21}$$

, where A is the cross-sectional area of interest, A^* is the cross-sectional area where the flow is sonic, γ is the ratio of specific heats, and M is the Mach number at the section of interest.

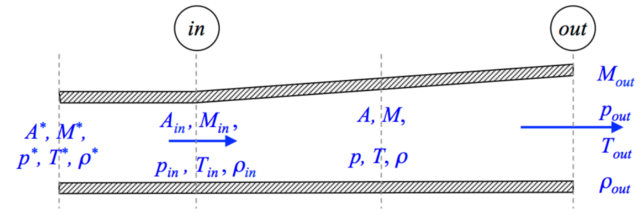

Figure 11. Confined expansion schematic.

2.4.6. Thrust Equation

Equation (22) gives the thrust generated by the scramjet is obtained by the momentum variation of the flow and pressure forces from the inlet to the exhaust region (Anderson, 2012).

$$T = \left(\dot{m}_0 + \dot{m}_f\right)V_e - \left(\dot{m}_0 V_\infty\right) + \left(p_e - p_\infty\right)A_e \tag{22}$$

, where $\dot{m}_0$ is the air mass flow rate, $\dot{m}_f$ is the fuel mass flow rate, V_e is the exhaust velocity in the longitudinal direction, V_∞ is the freestream velocity, p_e is the exhaust pressure, p_∞ is the freestream air pressure and A_e is the exhaust jet area.

2.4.7. Computation of Aerodynamic Forces

The aerodynamic forces on the 14-X S are basically drag and lift. Because 14-X S is symmetric along the longitudinal axis, lift should be always null for attack angle equal to zero. But, calculating the pressure distribution on the 14-X S due to shocks, combustion and expansion, it was possible to obtain the contribution of each surface (body, cowling and side plates) to the pressure drag. Also, given both coefficient of friction (c_f) and shear stress (τ_w) as a function of Mach and Reynolds numbers of the "outer" flow on each section, the friction can be computed. Finally, Eq. (23) gives the total drag (pressure and friction) per unit spam generated by each surface (Anderson, 1991).

$$D' = \int_{LE}^{TE}\left(-p_u \sin\theta + \tau_u \cos\theta\right)ds_u + \int_{LE}^{TE}\left(p_l \sin\theta + \tau_l \cos\theta\right)ds_l \tag{23}$$

, where, LE = leading edge; TE = trailing edge; p = pressure; τ = shear stress; u = upper surface; l = lower surface; and θ = inclination angle of the surface.

2.4.8. Van Driest Solutions

The Van Driest solutions for the laminar flow over a flat plate are presented in Fig. 12, where the friction coefficient is obtained as a function of both Mach and Reynolds numbers of the outer flow while the boundary layer thickness y depends on position x along the plate, and on both local Mach and Reynolds numbers.

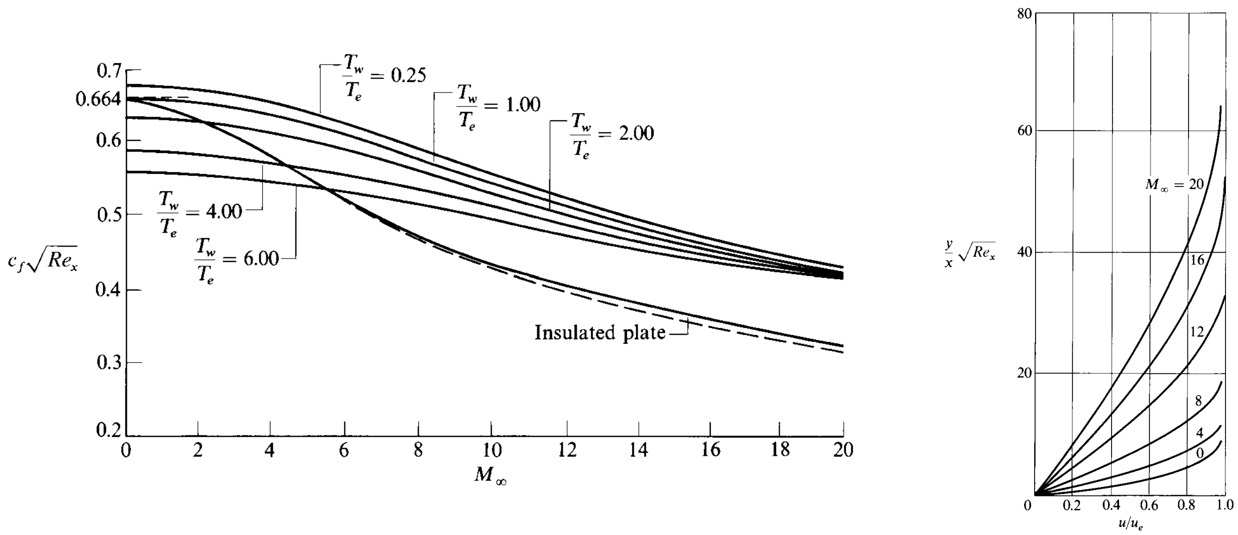

Figure 12. Van Driest solutions for friction coefficient and the boundary layer thickness (after Van Driest, 1952).

3. RESULTS

The Fig. 13 shows the pressure distribution obtained along the body and the cowling, where it is observed the peak of pressure due to combustion in sections C and 2.1.

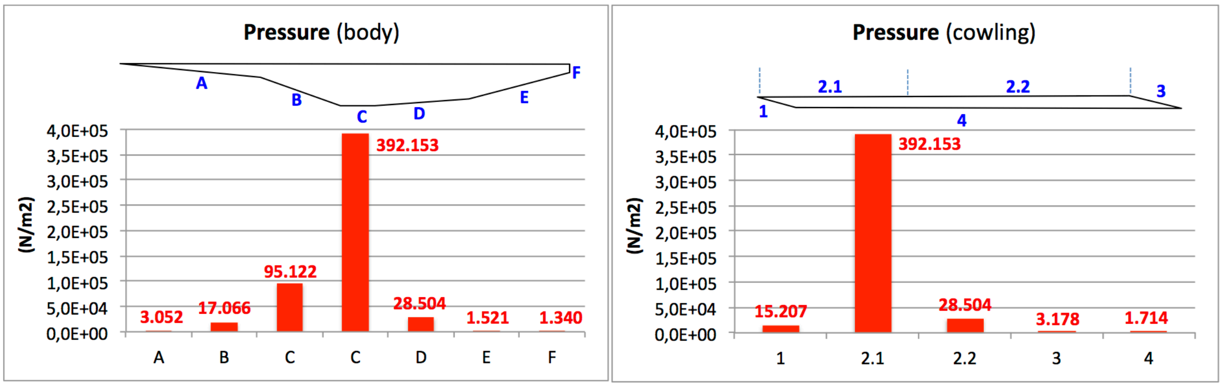

Figure 13. Pressure distribution throughout the body and the cowling of the 14-X S.

The pressure, viscous and total drags (pressure and viscous) for the body and cowling of the 14-X S (without considering the side plates) are shown in Fig. 14, where it is observed: the maximum pressure drag on the second compression ramp (section B); the friction is more pronounced in the internal expansion (sections D and 2.2); the pressure drag of the body is about 4,2 times higher than of the cowling, while the friction of the body is slightly longer than the fairing (18,58%); and, the main body produces about 3 times of the total drag over the cowling.

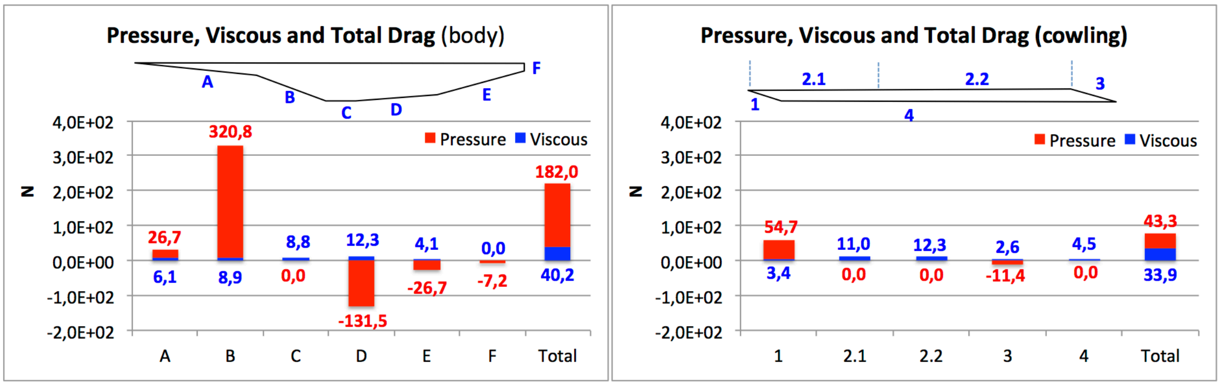

Figure 14. Pressure and viscous drag distribution on the body and cowling of the 14-X S.

In the case of the side plates of the 14-X S (Fig. 15), it is observed that externally there is pressure drag from 2,3 N (each) at P1 and P2, and of -0,4 N in P7 (rear), and the highest friction contribution happens in P5 (20,4 N); and, internally, obtains only friction, where the higher value takes place in LA and LE2 section (each 9,8 N). Also, it is observed that the pressure and friction drags due to the external flow (4,2 N and 44,2 N, respectively) are higher than those found for the internal flow to the plates (respectively, 0 N and 38,4 N).

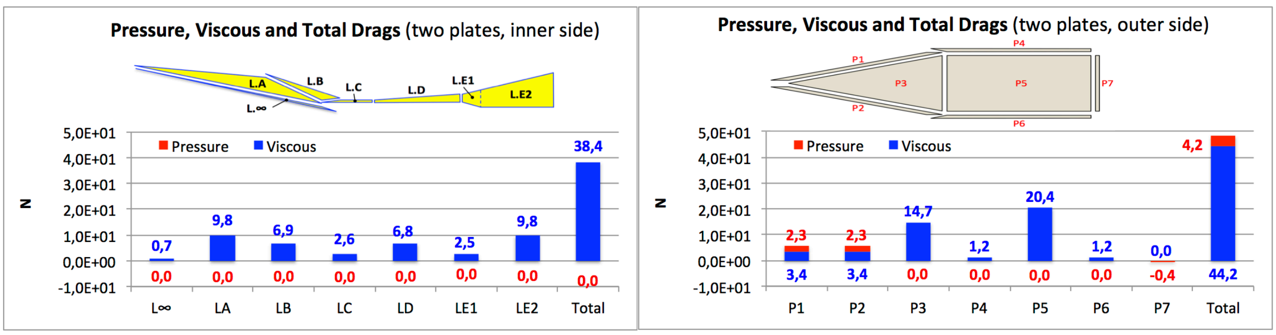

Figure 15. Pressure and friction drags distribution on the side plates (inner and outer sides).

The total drag of the 14-X S (body, cowling and side plates) totals 386,2 N, where 229,5 N due to wave (182 N body, 43,3 N cowling and 4,2 N side plates) and 156,7 N in the form of friction (40,2 N body, 33,9 N cowling and 82,6 N of the side plates – 38,4 N internally and 44,2 N externally).

The thrust computed for the 14-X S, as Eq. (21), totaled 273,7 N, where 258,5 N is due to the momentum addition and 15,2 N is due to the pressure increase, both caused by combustion, resulting in a liquid deceleration of 0,378 m/s^2. However, results not shown herein for thermally perfect gas assumption have revealed a net acceleration.

4. CONCLUSIONS

Under the 14-X flight research project, Brazil is aiming a flight test of the 14-X S scramjet engine in the near future. An aero-propulsive model based on high-temperature gas dynamic has been proposed for the 14-X S flying at 30 km of altitude and Mach number 7. For zero angle of attack, the lift generated by the 14-X S is null. For the ideal gas assumption, the model showed that the wave drag is maximum at the second ramp of compression (320,8 N) while the friction is larger at the internal expansion surface (12,3 N); 273,7 N of thrust is generated by 14-X S scramjet results in a small net deceleration of 0,378 m/s^2 because of the total drag of 386,2 N, where the main body contributes with 222,2 N, the cowlings with 77,2 N, and the side plates with 86,8 N. Also, the aerodynamic forces and thrust estimated herein will allow us to start exploring the flight dynamic of the 14-X S. As a future work, real gas effects (mainly, change in the ratio of specific heats with temperature), will be included in the current aero-propulsive model.

5. ACKNOWLEDGMENTS

The first author is grateful to the Air Force Command (COMAER), specifically the Institute of Advanced Studies (IEAv) for the research scholarship awarded.

6. REFERENCES

Anderson, J. D., Jr., 1991, “Fundamentals of Aerodynamics”, Ed. McGraw-Hill, New York, United States, 772 p.

Anderson, J. D., Jr., 2012, “Introduction to Flight”, Ed. McGraw-Hill, New York, United States, 925 p.

Anderson, J. D., Jr., 1990, “Modern Compressible Flow with Historical Perspective”, Ed. McGraw-Hill, New York, United States, 650 p.

Heiser, W. H. and Pratt, D. T. with Daley, D. H. and Mehta, U. B., 1994, “Hypersonic Airbreathing Propulsion”, AIAA, Washington, United States, 592 p.

Toro, P. G. P. *et al.*, 2012, “Brazilian 14-X Hypersonic Aerospace Vehicle Project”, 18th AIAA/3AF International Space Planes and Hypersonic Systems and Technologies Conference, France, AIAA 2012-5851.

Van Driest, E. R., 1952, “Investigation of Laminar Boundary Layer in Compressible Fluids using the Crocco Method”, NACA Technical Note 2597, Washington, United States, 79 p.

7. COPYRIGHT LIABILITY

MODELO AERO-PROPULSIVO DE UM DEMONSTRADOR TECNOLÓGICO SCRAMJET 14-X S: RESULTADOS PRELIMINARES

Sebastião de Carvalho Netto, scnetto27@hotmail.com[1]
Paulo Gilberto de Paula Toro, toro@ieav.cta.br[2]
Marco Antônio Sala Minucci, sala@ieav.cta.br[2]
Israel da Silveira Rêgo, israel.rego@ieav.cta.br[2]

[1]Instituto Tecnológico de Aeronáutica (ITA), Praça Marechal Eduardo Gomes, nº 50, Vila das Acácias, CEP 12.228-900, São José dos Campos/SP-Brasil.
[2]Instituto de Estudos Avançados (IEAv), Trevo Coronel Aviador José Alberto Albano do Amarente, nº 1, Putim, CEP 12.228-001, São José dos Campos/SP-Brasil.

Resumo: *Scramjets representam a última fronteira em motores aeronáuticos de alta velocidade. No laboratório de Aerotermodinâmica e Hipersônica Prof. Henry T. Nagamatsu do Instituto de Estudos Avançados (IEAv), é executada pesquisa e desenvolvimento de demonstradores tecnológicos de propulsão hipersônica aspirada baseada em combustão supersônica. Um desses é o scramjet 14-X S que será testado em voo a 30 km de altitude e velocidade equivalente a Mach 7, como um terceiro estágio aspirado de um motor foguete para acesso ao espaço. O scramjet 14-X S é um motor com simetria planar, onde cada metade possui duas rampas de compressão (inlet), uma câmara de combustão (combustor) e duas superfícies de expansão (tubeira) para a geração de tração. Este artigo apresenta um modelo para a determinação analítica das forças aerodinâmicas (arrasto e sustentação) e da força propulsiva (tração) que agem sobre o 14-X S em voo atmosférico hipersônico. O modelo aero-propulsivo aqui proposto considera o ar como gás caloricamente perfeito, atmosfera padrão para o escoamento livre, teoria de onda de choque para determinar os ângulos dos choques gerados pelo inlet (entrada de ar) do 14-X S e as propriedades através destes, teoria de Rayleigh para modelar a adição de calor devido à reação de combustão entre o fluxo de ar e o hidrogênio no combustor, teoria de expansão isentrópica (razão de áreas) para calcular as propriedades de exaustão através de regiões confinadas, teoria de Prandtl-Meyer para obter as propriedades do escoamento através de ondas de expansão centradas, e finalmente cálculo da tração. O efeito da viscosidade foi considerado através da mudança da geometria da entrada (inlet) e da tubeira do 14-X S e, assim, os ângulos de choque e expansão enquanto a fricção foi determinada através das soluções de Van-Driest para escoamento laminar. Os cálculos preliminares apresentam os seguintes resultados: o arrasto de pressão é máximo na segunda rampa de compressão do 14-X S; a fricção é mais pronunciada na seção da primeira expansão; o arrasto de onda global é maior que a fricção total; a tração gerada pelo motor é menor que o arrasto total, produzindo uma pequena desaceleração do 14-X S; e o corpo principal do 14-X S produz mais arrasto que sua carenagem.*

Keywords*: scramjet, cargas aerodinâmicas, hipersônica, voo de teste.*